JOURNAL OF PROPULSION AND POWER
Vol. 16, No. 6, November–December 2000

# Broadband Infrared Absorption Sensor for High-Pressure Combustor Control

J. M. Seitzman* and B. T. Scully†
*Georgia Institute of Technology, Atlanta, Georgia 30332-0150*

**A sensor approach for monitoring temperature uniformity, and also integrated water mole fraction, in the exit plane of a high-pressure gas turbine combustor is presented. The sensor, intended for use in an active control system, is based on infrared line-of-sight absorption measurements of water with a relatively broadband light source. Performance of the sensor was simulated using a computer model based on the HITRAN/HITEMP database for the infrared absorption of water. Specific regions of interest near 2.5 $\theta$ m were identified, based on their relative sensitivity to temperature. One region is relatively insensitive to temperature and permits monitoring of integrated water mole fraction across the exhaust. Two wavelengths, one with positive slope sensitivity and the other negative, are used to monitor the uniformity of the exhaust temperature profile. The linearity and sensitivity of the approach to uncertainties in the spectral shape and width, as well as the wavelength of the filtered light source, are also presented.**

## Introduction

FOR improved efficiency, gas turbine combustor designs call for progressively higher operating pressures. This is true for ground power systems and particularly appropriate for aeroengines. Simultaneously, there is growing interest in control strategies for optimizing performance across a range of operating conditions. These control systems are intended to improve performance of gas turbine combustors in a variety of areas, including pollutant emissions and combustion efficiency. Additionally, the high stresses and high temperatures that turbine blades encounter require maintenance of optimum turbine inlet conditions. For example, sufficiently uniform temperature profiles may be necessary to ensure that excessively hot or cold pockets of gas do not impinge on the turbine blades. Likewise at high-stress regions near the blade roots, lower temperature gases may be needed to prevent blade damage. The need for active control is especially important as engines become smaller and are obliged to achieve optimal performance in off-design conditions and under the course of normal engine wear.

Although active control of jet engine combustors offers great potential for such improvements, it requires sensors that are capable of monitoring performance parameters in high-temperature and high-pressure gases. For example, thermocouples are routinely employed for engine temperature measurements, for instance, in second stage turbine stators. However, the temperatures that exist at the combustor exhaust prevent thermocouples from successfully being employed ahead of the first turbine stage. In such a hostile environment, optical techniques are a natural solution because they offer the possibility of nonintrusive measurements. In particular, line-of-sight absorption based on infrared (IR) diode lasers has shown particular promise.[1,2] In general, the IR or near-IR lasers interact with rotational–vibrational transitions of a molecule. Strategies for simultaneous determination of gas concentration and temperature have been developed[3] and utilized for control of simple combustion devices.[4]

Current laser-based approaches have been limited, however, by the small wavelength range accessible by available laser sources. Single lasers can be tuned over small spectral regions; thus, appropriate sensors may involve a number of laser sources. Also, laser sources are not always available in regions that coincide with desired absorption features of the molecules of interest. Furthermore, the need for spectrally narrow laser sources is diminished at high pressures. Because diode lasers generally have a spectral output that is much narrower than the spectral lines of molecules, they are able to resolve single absorption lines. At high pressures, however, the molecular absorption features broaden to an extent that individual lines begin to disappear; the wings of one line overlap neighboring lines. Thus at elevated pressures, absorption sensors based on spectrally broader light sources have been suggested.[5]

We present a sensor strategy for monitoring conditions at the exit plane of a high-pressure gas turbine combustor. The strategy is based on a spectrally broad, but potentially tunable, light source and line-of-sight absorption measurements of water. Specifically, we consider approaches for monitoring temperature uniformity at the exit of the combustor (or entrance to the first-stage turbine) and also water mole fraction, as a gross measure of overall combustor health. Water was chosen from among the other likely candidates, that is, $CO_2$ and CO, because of its strong absorption features and because spectral regions exist with negligible gas absorption interferences from other important species. To test the sensor concept, we have simulated the sensor performance for typical aeroengine combustor exhaust conditions. The simulations are based on a model of the water absorption at elevated pressures.

## Absorption Modeling

To simulate the performance of the absorption sensor, the IR absorption features of water were modeled using a standard approach. First, the spectral absorption coefficient $k_\nu$ (units of per length) for a gas mixture at given thermodynamic conditions, including composition, is given by

$$k_\nu = \frac{p}{kT} \sum_i \chi_i \sum_j S_{ij}(T)\phi_{ij}(\nu - \nu_{ij}, T, p, \chi_i) \qquad (1)$$

where $k$ is Boltzmann's constant, $p$ and $T$ are the gas pressure and temperature at the point, $\chi_i$ is the mole fraction of the ith gas species with an absorption transition centered at frequency $\nu_{ij}$ having a line strength $S_{ij}(T)$ and line shape function $\phi_{ij}(\nu, T, p, \chi_i)$. The summations in Eq. (1) represent the contributions from multiple transitions $j$ and absorbing species $i$.

For a low-intensity light source with a center frequency of $\nu_0$ and a total intensity $I_0$, the total absorbance $A(\nu_0)$ a through a nonuniform

Received 5 June 1999; accepted for publication 22 November 1999. 

*Assistant Professor, Aerospace Combustion Laboratory, School of Aerospace Engineering.

†Graduate Research Assistant, Aerospace Combustion Laboratory, School of Aerospace Engineering.

gas mixture of length $L$ is then given by a form of the Beer–Lambert law,

$$A(\nu_0) = 1 - \int_{-\infty}^{\infty} \frac{I_\nu(L)\,\mathrm{d}\nu}{I_0} = 1 - \int_{-\infty}^{\infty} g(\nu) \exp\left[\int_0^L -k_\nu(x)\,\mathrm{d}x\right]\mathrm{d}\nu \tag{2}$$

where $I_\nu(L)$ is the spectral intensity at frequency $\nu$ after propagation of the incident light (at $x = 0$) to $x = L$, and where $k_\nu(x)$ is the spectral absorption coefficient at a distance $x$ from the source and $g(\nu)$ is the normalized incident spectral distribution of the light source defined by

$$g(\nu) = \frac{I_\nu(x=0)}{\int_{-\infty}^{\infty} I_\nu(x=0)\,\mathrm{d}\nu} = \frac{I_\nu, 0}{I_0} \tag{3}$$

The more traditional form of the Beer–Lambert law is recovered for a uniform distribution across the path; that is,

$$\frac{I(L)}{I_0} = 1 - A(\nu_0) = \int_{-\infty}^{\infty} g(\nu) \exp[-k_\nu L]\,\mathrm{d}\nu \tag{4}$$

For the modeling presented here, the line strength information was obtained from the HITEMP database, a high-temperature version of the HITRAN database for selected molecules, in conjunction with the HAWKS computer software.[6,7] The spectral line shapes were assumed to be Voigt functions (see Ref. 8), a combination of Doppler broadening and collision broadening. Although collisional narrowing and line shifts are likely to occur at high pressures,[9,10] such effects have been neglected in these calculations. Because these effects are typically much less than the nominal value of the collisional broadening, they should not be important for the current simulations, which assume a light source much broader than the spectral width of the absorption features. The collisional broadening information was also obtained from HITEMP.

Equations (1) and (2) show that the total absorbance of the gas generally depends on the composition, temperature, and pressure of the gas, through $k_\nu(x)$. Thus, with appropriate selection of measurement frequencies, it is possible to monitor these variables. Because the absorbance depends on the distribution of $k_\nu$ integrated across the path, however, any resulting measurement must be recognized as some path-averaged property, which depends on the combined distributions of the composition, temperature, and pressure across the path. In other words, the absorbance depends on path-dependent correlations between the properties. For example, a temperature inverted from an absorption measurement, for example, through a Boltzmann ratio of the absorbance at two wavelengths, will typically be different than a mass-averaged temperature across the path due to the correlation between temperature and absorber mole fraction across the path and the nonlinearity of Eqs. (1) and (2).

When spatially resolved measurements are required in nonuniform flows, this path averaging may represent a significant problem and require complex reconstructional algorithms.[11] The measurement requirements of a sensor used for active control can, however, be less demanding. For example, a reasonable estimate of the average value of water mole fraction or temperature at the combustor exit can be sufficient to monitor the health of the combustor.

## Exhaust Conditions and Band Selection

To identify a strategy for water sensing in the exhaust plane of a gas turbine combustor, the following conditions were considered. Across the exit, local gas temperatures were assumed to be within the range 700–2100 K, with pressures in excess of 5 atm. For much of the modeling, a nominal pressure of 10 atm, constant across the exhaust, was used. Pressures in excess of 5 atm and the temperature range given are reasonable values for modern, high-pressure-ratio aircraft turbine engines at a range of altitudes and operating conditions. Additionally, the exhaust composition assumes comparable water and carbon dioxide mole fractions, which is appropriate for jet fuels with C:H ratios near 1:2. For the purposes of this investigation, the sensor was assumed to integrate over a 10-cm path length. This is similar to the distance across common annular combustors. Additionally, the sensor's light source/detector system was assumed to be have a spectral profile given by a Lorentzian with a resolution [full-width at half-maximum (FWHM)] of 10 $\mathrm{cm}^{-1}$. The Lorentzian profile, with its extensive wings, was chosen to simulate a light source that employs a spectral bandpass filter with good, but finite, out-of-band rejection.

There are a number of regions in the IR that exhibit noticeable absorption due to water. For reasons related to thermal background emission, detector performance, and absorption in optical materials, we restrict our consideration to wavelengths less than about 3 $\mu$m, or frequencies greater than about 3300 $\mathrm{cm}^{-1}$. In this range, the absorption features of water can be divided into three distinct regions. For 3000–4000 $\mathrm{cm}^{-1}$ (3.3–2.5 $\mu$m), the dominant features result from two fundamental transitions: specifically, transitions from the ground level to two excited vibrational levels, (1, 0, 0) and (0, 0, 1). For the two other regions, 4800–5800 $\mathrm{cm}^{-1}$ (2.1–1.7 $\mu$m) and 6800–7600 $\mathrm{cm}^{-1}$ (1.5–1.3 $\mu$m), combination bands primarily contribute to peak absorption levels about one order of magnitude weaker than for the fundamental bands. Note that it is in the latter, short wavelength region that most diode-laser measurements of water have been conducted.[2–4,10,12,13]

For the conditions at the combustor exhaust, all three regions offer potential for broadband water sensing. From the standpoint of interferences due to absorption by other major gas constituents, primarily $CO_2$, most of the 7000-$\mathrm{cm}^{-1}$ band is virtually problem free. Regions of the other bands can also be found with little or no $CO_2$ interference.[5] For example, the region above 3800 $\mathrm{cm}^{-1}$ is free of $CO_2$ interference. Strong absorbances, which provide better data from a signal-to-noise perspective, are more easily found in the strongly absorbing 3000–4000 $\mathrm{cm}^{-1}$ region. However, absorbances above 0.01 can also be found for the other regions.

Finally, it is important to find spectral regions with low absorbance for background/baseline corrections. For sensors that must operate in real or dirty environments, the possibility of scattering particles or degradation of optics must be considered. This requires the ability to record the transmitted light intensity in spectral regions with little or no gas absorption. Because these background sources of light extinction are not uniform over large wavelength ranges, the regions of low absorption should be as close to the measurement wavelength as possible. It is this last constraint, along with the lack of $CO_2$ interferences, that led us to focus currently on the region above 3800 $\mathrm{cm}^{-1}$. The other water absorption bands, however, also hold promise for sensors based on the approaches described next.

## Results

### Spectra

Spectral absorption coefficients were calculated according to Eq. (1). The summation over spectral lines was performed for all transitions with center frequencies within 16 $\mathrm{cm}^{-1}$ of the desired frequency. This is at least 40 times greater than the half-width of the transitions at the conditions of interest, and calculations with greater summation ranges yield effectively identical results. Figure 1 illustrates the effect high pressures on the absorption coefficients of water. As already suggested, the collision broadening of individual transitions at 10 atm causes them to merge, and recognizable absorption features actually consist of multiple absorption lines. This becomes even more pronounced at higher operating pressures. Whereas a light source with a relatively narrow spectral output is needed to resolve single absorption features at 1 atm, a much broader source can be used at higher pressures. At high pressures, the extensive broadening also makes it more difficult to find regions between lines that have sufficiently low absorption for correcting background absorption.

These high-pressure spectral absorption coefficients were then used to calculate total absorbances for a 10-$\mathrm{cm}^{-1}$ bandwidth (Lorentzian) light source over a 10-cm path and a water mole fraction of 0.05, according to Eq. (2). The integration over frequency

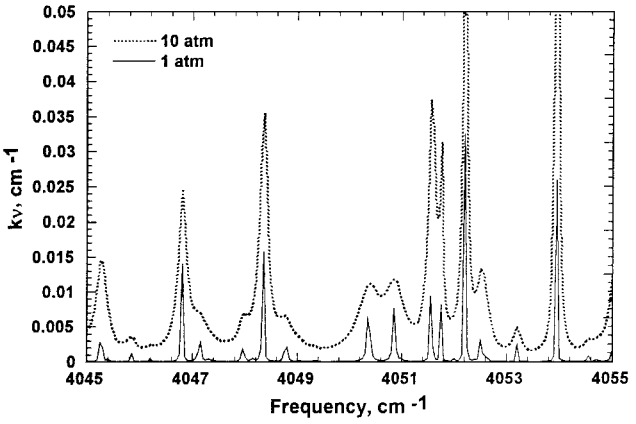


**Fig. 1 Spectral absorption coefficient $k_\nu$ for a mixture containing 5% water by mole at 1300 K for two pressures, 1 and 10 atm.**

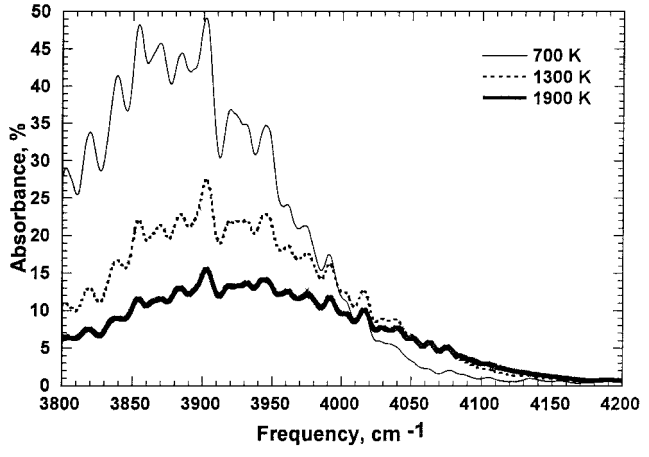


**Fig. 2 Total absorbance for a broadband (10-cm$^{-1}$) light source over a 10-cm path length in a uniform gas at 10 atm, 5% $H_2O$ by volume.**

was carried out over a range 10 times greater than the FWHM of the light source; again larger integration ranges did not yield significantly different results. Figure 2 shows the total absorbances for three temperatures over a frequency range of 3800–4200 cm$^{-1}$. We note that, over most of this range, the absorbances are above 0.01, which is desirable for ensuring reasonable signal-to-noise ratio measurements. In the region beyond 4300 cm$^{-1}$, the absorbance falls below 0.004 for temperatures below 1600 K. Thus, background corrections, for example, for scattering, could be made there. Figure 2 also shows that the broadband absorbance has a noticeably different temperature dependence in three regions. At low frequencies, nearer 3800 cm$^{-1}$, the absorbance decreases with increasing temperature, whereas above 4100 cm$^{-1}$, the absorbance increases. In a central region, near 4010 cm$^{-1}$, the temperature dependence of the absorbance is greatly reduced.

### Water Mole Fraction Sensing

As already noted, overall combustor performance, for example, gross degree of fuel conversion, can be roughly quickly monitored by sensing the total water content in the gases at the combustor exhaust. In general, however, the absorbance depends nonlinearly on the combination of pressure, water mole fraction, and temperature distributions across the path [see Eqs. (1) and (2)]. What we would like to find is a situation in which the absorbance is only a function of water mole fraction. Often, the pressure is nearly constant through a cross section of the flow and, if necessary, could be measured by sensors monitoring the pressure at the combustor wall. Therefore, we

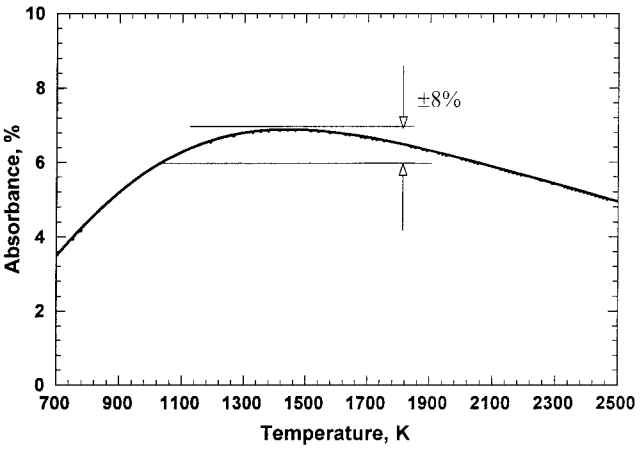


**Fig. 3 Temperature (in)sensitivity of the broadband absorbance for a 10-cm$^{-1}$ light source centered at 4049 cm$^{-1}$ and passing through 10 cm of a uniform gas mixture, 5% $H_2O$ by volume, and at 10 atm.**

need only focus on the temperature dependence of the absorbance. What we desire is a spectral region where the absorbance is (nearly) independent of temperature. As seen in Fig. 2, there is such a region with weak temperature dependence around 4000 cm.$^{-1}$

For example, Fig. 3 shows the temperature dependence of the absorbance for a light source centered at 4049 cm$^{-1}$. Compared to other frequencies, a light source centered here has a relatively small change in absorbance (±8%) for a constant mole fraction of water over the temperature range 1000–2100 K. Thus, integrated water fraction measurements could be made to a ±8% relative accuracy under these conditions. A sensor with this accuracy should be adequate for use in an active control system monitoring overall combustor health. For water colder than 1000 K, the temperature sensitivity at 4049 cm$^{-1}$ increases. For example, the absorbance varies by ±15% over the range 900–2400 K. For better temperature insensitivity to cold gases, a position closer to 4000 cm$^{-1}$ would be appropriate (see Fig. 2); on the other hand, the temperature sensitivity at higher temperatures would increase.

Whereas temperature insensitivity is one requirement for an absorption sensor intended to monitor water content at the combustor exhaust, there are other equally important sensitivity/uncertainty issues to be considered. As seen in Eq. (2), the absorbance depends exponentially on absorber mole fraction. For simplified data reduction, it is advantageous for the absorbance to depend nearly linearly on mole fraction, rather than through the exponential relationship of Eq. (2). By the examining of the simple case of a uniform distribution across the path [Eq. (4)],

$$A(\nu_0) = 1 - \int_{-\infty}^{\infty} g(\nu) \exp[-k_\nu L]\, d\nu$$

$$\cong \int_{-\infty}^{\infty} g(\nu)[k_\nu L]\, d\nu \propto k_\nu \propto \chi_{H_2O} \tag{5}$$

where the removal of the exponential is strictly valid when the term in brackets is small ($\ll$1) for all frequencies in the bandwidth of the light source. In this case, the absorbance is essentially a linear function of the water content in the measurement volume. Figure 4 shows the variation in absorbance with water level, for a constant temperature of 1300 K and pressure of 10 atm. The absorbance reaches nearly 0.12 for $\chi_{H_2O} = 0.09$ and exhibits a slightly less than linear increase with water content for $\chi_{H_2O} > 0.05$. The relative error, $|A(\nu) - A'(\nu)|/A(\nu)$, where $A(\nu)$ is the computed absorbance and $A'(\nu)$ is a best-fit approximation to the absorbance (solid line), is no more than 7% for a linear fit up to $\chi_{H_2O} \cong 0.07$. For improved accuracy, a quadratic best fit gives a relative error less than 2% over the complete range of water mole fractions shown (dashed line).

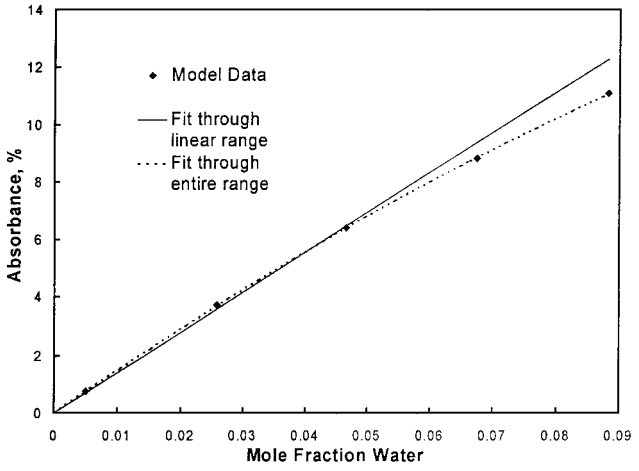


**Fig. 4 Variation in total absorbance with water mole fraction for a 10-cm$^{-1}$ light source centered at 4049 cm$^{-1}$ for uniform combustor exhaust conditions of 10 atm, 1300 K, and a 10-cm path length.**

Thus, simple relationships can be effectively used to convert measured absorbance to water mole fraction. This may seem surprising, considering that the peak spectral absorption coefficients in this region are near 0.1 or $k_\nu L$ is of the order one. This is beyond the range where the exponential term in brackets in Eq. (5) can be linearly approximated; that is, $\exp(-k_\nu L) \cong (1 - k_\nu L)$. As seen in Fig. 1, however, much of the absorption for a broadband (10-cm$^{-1}$) source occurs in the wings (weaker regions) of the absorption lines, and thus the linear approximation remains valid for a broadband sensor and moderate amounts of water.

We also investigated the accuracy of the water sensor response to potential uncertainties in other parameters, including the source profile, center frequency shifts, and absorption line broadening. The sensitivity of the water sensor to uncertainties in collisional broadening of the water lines is considered first. Collision broadening is generally considered to be linearly proportional to pressure and to vary with temperature to some power.[2,4,6] Unfortunately, the temperature scaling of the water broadening is not well characterized for all of the transitions of importance.[3,14] In accord with the HITEMP database, the temperature scaling exponent for most of the transitions examined was approximately 0.5–0.7. To test sensitivity to temperature scaling, simulations were performed with no temperature scaling, which effectively increases the broadening. Only results for the narrowband (source) case were noticeably altered. Because the spectral extent of the broadband source is quite large compared to even the broadened absorption features, the broadband source is less sensitive to line broadening effects. Similarly, we investigated the sensitivity of the water sensor to potential uncertainties in the exact center frequency of the light source and its spectral distribution. We compared the predicted absorbances of a sensor using the nominal sensor parameters, for example, 10 cm$^{-1}$ FWHM, to absorbances produced using up to a $\pm$2-cm$^{-1}$ shift in the center frequency combined with variations in the widths of the distribution of $\pm$3 cm$^{-1}$ ($\pm$30% in FWHM). With these effects combined, the relative change in absorbance was less than ~6%. We also tested a change in the distribution from a Lorentzian to a Gaussian. The Gaussian, which has wings that decay much faster than the Lorentzian, produced a relative change in absorbance of 12%.

In summary, we find that a broadband absorption sensor looks promising as a means for monitoring water mole fraction. According to the modeling, this can be done with only a weak dependence on gas temperature. Furthermore, in most cases a simple linear (or perhaps quadratic) relationship between absorbance and water mole fraction can be used for simplified data reduction. Finally, reasonable uncertainties in line broadening, detection bandwidth, and detection frequency do not have significant impact on the sensor response.

Note, however, that like all path-averaged measurements, the path-average result $\bar{\chi}$ is not necessarily equal to the more conventional (density-weighted) averaged $\tilde{\chi}$ over the measurement volume; that is,

$$\bar{\chi}_{H_2O} \equiv \int_0^L \chi_{H_2O}(x)\,dx \neq \tilde{\chi}_{H_2O} \equiv \int_0^L n_{H_2O}(x)\,dx \Big/ \int_0^L n_{tot}(x)\,dx$$

$$= \int_0^L \chi_{H_2O}(x) n_{tot}(x)\,dx \Big/ \int_0^L n_{tot}(x)\,dx$$

$$= \int_0^L \frac{\chi_{H_2O}(x)}{T(x)}\,dx \Big/ \int_0^L \frac{1}{T(x)}\,dx \qquad (6)$$

where $n(x)$ is the number of moles and where the last step assumes a uniform pressure across the path. The difference between $\bar{\chi}_{H_2O}$ and $\tilde{\chi}_{H_2O}$ depends on the temperature (or molar concentration in the most general case) variation across the path. This leads to the problem of sensing the level of nonuniformity across the measurement path.

### Temperature Uniformity Sensing

As already noted, uniformity of the temperature across the combustor exit is an important performance parameter for gas turbines. Excessively high or low temperatures can impact the structural integrity of highly stressed turbine blades that are just downstream of the combustor. Unlike sensing of water mole fraction, temperature sensing requires a region of the absorbance spectrum that is sensitive to temperature variations. This can be accomplished with absorption measurements in either of the other two regions shown in Fig. 2. In the region near 3800 cm$^{-1}$, the absorbance decreases with temperature, whereas above ~4100 cm$^{-1}$ it generally increases (although the absolute variation in absorbance is not large in this spectral region, the fractional change is significant).

Based on the modeled temperature dependence, absorbance measurements near 3800 cm$^{-1}$ will be more heavily weighted toward portions of the flow containing cold water, and measurements near 4100 cm$^{-1}$ are more sensitive to parts of the exhaust that contain hot water. From a mathematical viewpoint, the temperature weighting is clearly evident in the linear limit of Eq. (2) (this limiting assumption is not necessary to the argument, but simply helpful in the explanation),

$$A(\nu_0) = \int_0^L \chi_{H_2O}(x) f_{\nu_0}[T(x)]\,dx \qquad (7)$$

where $f_{\nu_0}(T)$ is the temperature dependence of the absorbance for the light source centered at $\nu_0$ and we have assumed a fixed and known pressure. Now it is easily seen that the integral, and therefore the absorbance, for a given center frequency will be weighted toward spatial locations with high values of $f_{\nu_0}(T)$.

The uniformity of the temperature profile across a path can be found by comparing the absorbance at a few spectral positions $\nu_i$, if $f_{\nu_i}(T)$ is appreciably different for each $\nu_i$. For example, in the linear limit, we could determine a path-averaged temperature by taking the ratio of the absorbance in the cold-sensitive region to that in the temperature-insensitive region; that is,

$$\frac{A(3800\,\text{cm}^{-1})}{A(4049\,\text{cm}^{-1})} \cong \frac{\int_0^L \chi_{H_2O}(x) f_{3800}[T(x)]\,dx}{\int_0^L \chi_{H_2O}(x) f_{4049}[T(x)]\,dx}$$

$$\cong \frac{1}{f_{4049}\bar{\chi}_{H_2O} L} \int_0^L \chi_{H_2O}(x) f_{3800}[T(x)]\,dx \qquad (8)$$

where for simplicity of the explanation, we have assumed that the 4049-cm$^{-1}$ absorbance has no temperature dependence and yields

$\bar{\chi}_{H_2O}$. An effective average temperature $\bar{T}_{3800}$ could then be produced by inverting the result

$$\bar{T}_{3800} = f_{3800}^{-1}\left[\frac{A(3800\,\mathrm{cm}^{-1})}{A(4049\,\mathrm{cm}^{-1})}\right] \cong f_{3800}^{-1}\left[\frac{A(3800\,\mathrm{cm}^{-1})}{f_{4049}\bar{\chi}_{H_2O}L}\right] \quad (9)$$

where $f^{-1}$ is the inverse function of $f$. Effectively, this procedure gives a temperature that corresponds to a uniform gas with the same absorption and path-averaged (rather than density-averaged) water content as the actual profile. Similarly, measurements near 4100 $\mathrm{cm}^{-1}$ could be used to produce another temperature $\bar{T}_{4100}$. Because $\bar{T}_{4100}$ is more sensitive to parts of the exhaust that contain hot water and $\bar{T}_{3800}$ is weighted toward the cold gas regions, we find in general that $\bar{T}_{4100} > \bar{T}_{3800}$. Thus, a comparison of the temperatures predicted by the two measurements would be a test of a flow's temperature uniformity. As shown later, the difference in the two temperatures can also be used as a measure of the degree of deviation from a uniform profile. This difference signal could then be used in a feedback loop of an active control system devoted to maintaining a (nearly) uniform temperature profile.

Two specific spectral locations, 3816 and 4104 $\mathrm{cm}^{-1}$, were identified as appropriate for temperature uniformity monitoring. Both have reasonable absorption levels and show a strong, monotonic response to temperature variations across the range 700–2000 K. The effective temperatures resulting from measured absorbances at these wavelengths were simulated for two temperature profiles. The first case was a uniform path, 10 cm long, containing 1300-K gas. The nonuniform case was a bimodal distribution containing 3.8 cm of 1000-K gas and 6.2 cm of 1600-K gas. For the comparison, both profiles have the same total path (10 cm), same $\bar{T}$ (1300 K), and a constant $\chi_{H_2O}$ (0.05). For illustrative purposes, the temperatures ($\bar{T}_{cold}$ from the 3816 $\mathrm{cm}^{-1}$ result and $\bar{T}_{hot}$ for 4104 $\mathrm{cm}^{-1}$) were inverted from the simulated absorbances and the known $\chi_{H_2O}$. As expected, both temperatures inverted for the uniform profile are close to 1300 K, $\bar{T}_{cold} = 1299$ K and $\bar{T}_{hot} = 1302$ K, with the difference due to the simulated noise floor for the absorbance. For the nonuniform case, $\bar{T}_{cold}$ and $\bar{T}_{hot}$ were significantly different: 1228 and 1326 K, respectively.

### Simulated Sensor Performance with Water/Temperature Correlation

To this point, all calculations were based on independent values for water mole fraction and temperature. For a combustor exhaust, this is unrealistic; there will be some correlation between water content and temperature. For instance, high-temperature regions will tend to consist of hot combustion products, including high water content, that have not mixed with much of the colder, drier dilution air from the compressor.

To investigate the importance of such a relationship, we considered a simple linear correlation between temperature and water content. For purposes of the simulations to be discussed, we obtained the linear correlation by taking the gas at any point in the combustor exhaust to be a mixture of stoichiometric combustion products and dilution air. The adiabatic flame temperature of a stoichiometric mixture of jet fuel burning with preheated air was taken to be 2500 K, and the products contain 13% water. For the nominal conditions of the dilution air, we assumed a temperature of 700 K and 0.5% water. At both these extremes, the molecular weight of the gas is nearly identical. For any intermediate mixture, we assume a linear relation between temperature and water content. Essentially, this requires constant specific heats, complete combustion, and no heat losses. Although none of these assumptions is completely valid, they are sufficient to test the behavior of the proposed sensor approach in a nonuniform combustor exhaust.

The overall influence of the water–temperature is seen in Fig. 5, which shows the total absorbances for the same conditions used in Fig. 2. Now, the absorbances are weighted more toward hot gases, which contain higher levels of water. The water content at each temperature varies linearly with temperature. Specifically, the region near 4100 $\mathrm{cm}^{-1}$ shows a much greater sensitivity to hot gases, that is, an increased absorbance with temperature rise. Conversely, the region previously weighted toward cold gases (below 3900 $\mathrm{cm}^{-1}$, see Fig. 2) has a much reduced sensitivity. In fact, the effects of the water–temperature correlation nearly offset the (fixed-water) temperature sensitivity above about 1000 K.

**Table 1 Simulated water mole fraction measurement results**

| Profile | Absorbance | Measured $\bar{\chi}_{H_2O}$ | Error, % | Calculated $\bar{\chi}_{H_2O}$ |
|---|---|---|---|---|
| Uniform | 0.064 | 0.046 | −1.5 | 0.0467 |
| Partial mixing | 0.068 | 0.049 | 4.9 | 0.0515 |
| Cooling layer | 0.075 | 0.054 | 15.6 | 0.0563 |
| Hot spike | 0.065 | 0.047 | 0.6 | 0.0501 |
| Cold spike | 0.070 | 0.050 | 7.1 | 0.0520 |

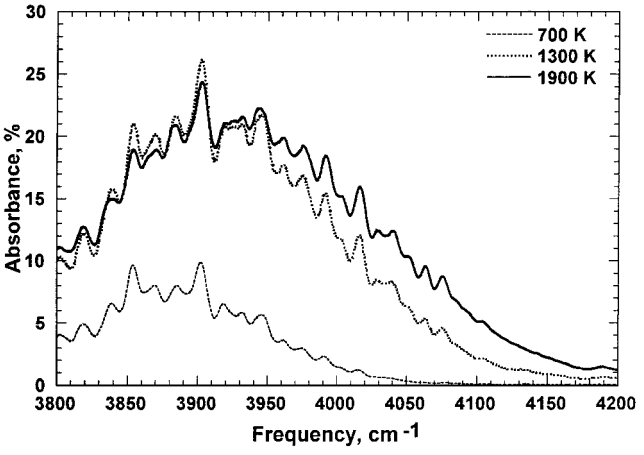


**Fig. 5 Total absorbance for broadband light source over a 10-cm path in a uniform gas at 10 atm and various temperatures.**

Based on the described water–temperature correlation, simulations were performed for a broadband sensor intended to monitor integrated water mole fraction and temperature uniformity in a combustor exhaust. The simulations were performed by calculation of the total absorbances that would be obtained for various exhaust gas profiles (Fig. 6). In each, the temperature range at the combustor exhaust was limited to 700–2000 K. The lower limit allows for residual (pure) dilution air (though preheated by the compressor) to be present at the exhaust, whereas the upper limit presupposes some mixing of the products of any stoichiometric combustion that could have occurred. Each profile represents a path containing the same (density-weighted) overall water content, $\tilde{\chi}_{H_2O} = 4.67\%$, and temperature, $\bar{T} = 1300$ K. The profiles include 1) a single stream (uniform), 2) a bimodal distribution with both streams close to the uniform conditions (partial mixing), 3) a bimodal distribution with a mixed stream and small regions of pure dilution air that might be residuals of the cooler flow used to protect a casing or liner (cooling layer), and two trimodal distributions with a small region of poor mixing containing either very 4) hot gases (hot spike) or 5) cold gases (cold spike).

Table 1 contains the calculated absorbances for each of the listed gas profiles shown in Fig. 6 at pressure of 10 atm for a sensor with a 10-$\mathrm{cm}^{-1}$-wide Lorentzian light source centered at a low-temperature sensitivity position (4049 $\mathrm{cm}^{-1}$). The calculated absorbances are all rounded to the nearest 0.001 to simulate a sensor resolution of $10^{-3}$ in absorbance. Also shown are the mole fractions that would be inferred from the rounded absorbances, based on the linear fit of Fig. 4. For the uniform profile, the inferred mole fraction is 0.046, which is 1.5% below the expected value of 0.0467. The error results primarily from the difference between the linear fit and the actual absorbance change with water mole fraction. Compared to the uniform profile, only the two profiles containing pure dilution air (cooling layer and cold spike) produce significant errors in integrated water fraction. Additionally for all the nonuniform profiles, the measured mole fractions $\bar{\chi}_{H_2O}$ are above the density-weighted value of 0.0467. Most of this error is due to the difference between

$\bar{\chi}_{H_2O}$ and $\tilde{\chi}_{H_2O}$. The second to last column shows the error between the measured mole fractions and the true density weighted average $\tilde{\chi}_{H_2O}$, and the last column provides the true values of $\bar{\chi}_{H_2O}$. For the correlation chosen here, that is, water level increasing with temperature, $\bar{\chi}_{H_2O} > \tilde{\chi}_{H_2O}$, as seen in the last column of Table 1. This difference is most evident for the cooling layer, which is at 700 K for nearly one-fifth of its length and has an error of nearly +16% compared to $\tilde{\chi}_{H_2O}$, but only −4% compared to $\bar{\chi}_{H_2O}$.

Table 2 lists the absorbance $A$ values calculated for the profiles of Fig. 6 that simulate a sensor with a 10-cm$^{-1}$-wide Lorentzian light source centered at the two temperature sensitive positions noted in the preceding section, with absorbances weighted toward cold (3816-cm$^{-1}$) and hot (4104-cm$^{-1}$) gases. For most cases, the change in absorbance at both frequencies, compared to the uniform distribution, is well above the 0.1% resolution assumed for a practical sensor. For the cooling layer and cold spike cases, measurements at both frequencies would record a significant difference from the uniform case. For the hot spike and partial mixing profiles, only the measurement sensitive to hot gases records a significant change. The reduced sensitivity of the cold weighted measurement results from offsetting effects of the temperature sensitivity and the water–temperature correlation as shown in Fig. 5. In any case, the overall result, for example the ratio of the hot and cold measurement positions, for the nonuniform cases, is significantly different from the uniform profile.

It is unlikely, however, that a control system would have a priori knowledge of the average gas temperature at the exhaust. Therefore, it could not compare the absorbances to an (unknown) uniform case to infer temperature uniformity. Rather, as prescribed by Eqs. (8) and (9), the sensor would infer two effective average temperatures, one based on the cold-weighted measurement and one based on the hot-weighted measurement. The effective temperatures $\bar{T}$ are inverted using the calculated variation of absorbance with temperature (at each measurement wavelength) assuming a uniform path of 10 cm. The two calibration curves are determined at one water concentration and linearly scaled by the integrated water concentration inferred from the temperature-independent line.

**Table 2 Absorbances simulations for temperature sensitive frequencies**

| Profile | $A$ (3816 cm$^{-1}$) cold | $A$ (4104 cm$^{-1}$) hot |
|---|---|---|
| Uniform | 0.116 | 0.021 |
| Partial mixing | 0.115 | 0.026 |
| Cooling layer | 0.107 | 0.031 |
| Hot spike | 0.115 | 0.024 |
| Cold spike | 0.111 | 0.027 |

Table 3 shows the temperatures inferred for the absorbance measurements listed in Table 2 based on two approaches using a known integrated water level and using a water level inferred from the temperature-insensitive line. In one case, no temperature can be inferred (NA). The effective temperature results based on the measured water content are shown in the rightmost columns of Table 3. In all cases, $\bar{T}_{hot}$ is above $\bar{T}_{cold}$. For the uniform case, both temperatures have a small error compared to the expected value of 1300 K. The temperature error comes mainly from the small error in the measured water content. Based on this result, the estimated sensor accuracy is 20 K at the simulated conditions (and for a uniform, steady flow). For the nonuniform profiles, the difference between the two effective temperatures, $\Delta T = \bar{T}_{hot} - \bar{T}_{cold}$, ranges from 125 to 233 K. Thus, the nonuniform profiles can easily be distinguished from the uniform case (with $\Delta T = 12$ K).

For both sensor outputs, hot and cold, the effective temperatures are above the true density-weighted temperature. This is in contrast to the constant mole fraction results, where only $\bar{T}_{hot}$ was above $\tilde{T}$. Now $\bar{T}_{cold}$ also exceeds $\tilde{T}$, predominantly due to the water–temperature correlation, that is, there is more water at higher temperatures. Thus, all effective $\bar{T}$ become more weighted toward hotter gases. As was seen in the absorbance values of Table 2, $\bar{T}_{cold}$ is nearly temperature insensitive for cases without very cold gases. Thus, $\bar{T}_{cold}$ is very close to $\tilde{T}$ except in cases where the profile contains completely unmixed air (700 K). This is mainly due to its effective temperature sensitivity including the water–temperature correlation. As seen in Fig. 5, the absorbance for the cold sensor (at 3816 cm$^{-1}$) is now weakly sensitive to temperature variations above ~1000 K. Below that value, the absorbance decreases as the temperature drops. Though the cold absorbance does not have the same weighting toward cold gases as it did for a fixed water content, our approach for monitoring temperature uniformity still works because we are sensing at two wavelengths with drastically different temperature sensitivities.

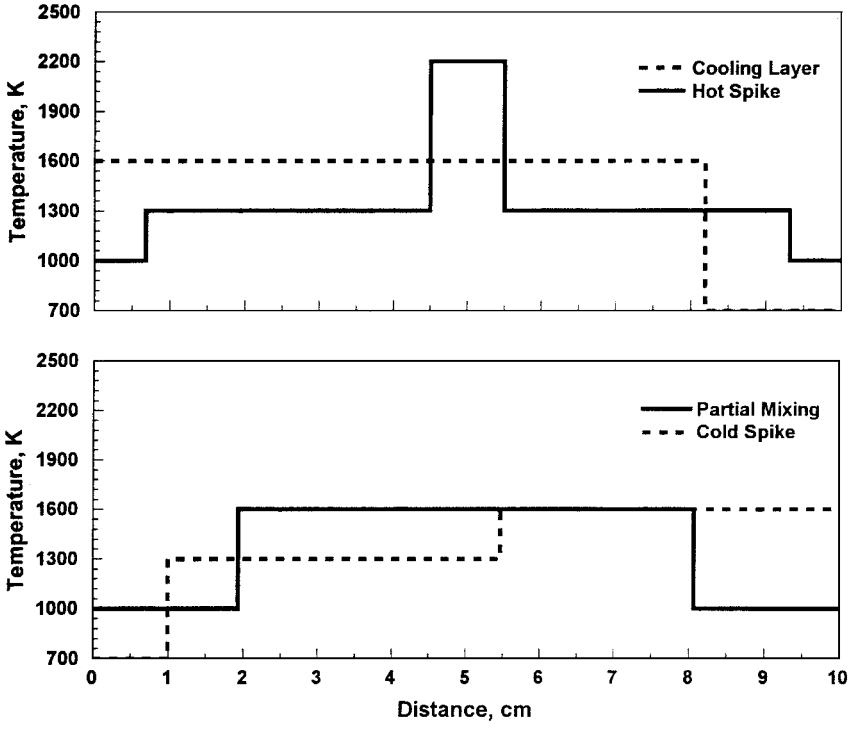


**Fig. 6 Test profiles of temperature across a 10-cm path through the exit plane of a combustor.**

**Table 3 Temperature uniformity sensing results**

| | $\bar{T}$ based on actual $\tilde{\chi}_{H_2O}$, K | | | $\bar{T}$ based on measured $\bar{\chi}_{H_2O}$, K | | |
|---|---|---|---|---|---|---|
| Profile | $\bar{T}_{cold}$ 3816 cm$^{-1}$ | $\bar{T}_{hot}$ 4104 cm$^{-1}$ | $\Delta T$ | $\bar{T}_{cold}$ 3816 cm$^{-1}$ | $\bar{T}_{hot}$ 4104 cm$^{-1}$ | $\Delta T$ |
| Uniform | 1295 | 1281 | 14 | 1285 | 1297 | 12 |
| Partial mixing | 1300 | 1609 | 309 | 1352 | 1530 | 178 |
| Cooling layer | 1381 | NA | NA | 1526 | 1759 | 233 |
| Hot spike | 1300 | 1475 | 175 | 1300 | 1475 | 175 |
| Cold spike | 1340 | 1781 | 441 | 1421 | 1546 | 125 |

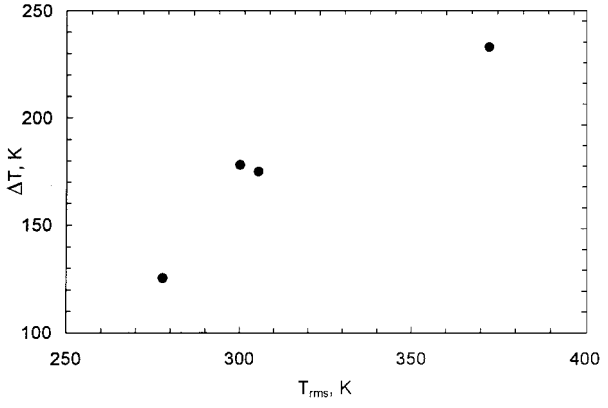


**Fig. 7 Relationship between differential sensor output, $\Delta T = \bar{T}_{hot} - \bar{T}_{cold}$, and $T_{rms}$ for the four nonuniform profiles shown in Fig. 6.**

The effect of using the temperature-independent line as a measure of the water content can be seen by comparing those results to temperatures inverted using the actual water content $\tilde{\chi}_{H_2O}$. These temperatures are found in the central columns of Table 3. When the actual, density-weighted water content is employed, $\bar{T}_{cold}$ provides an even better measure of the true $\tilde{T}$. For profiles that do not contain 700-K gases, the average temperature can be inverted quite accurately. In addition, the hot line is now more sensitive to nonuniformities. For the cooling layer case, $\bar{T}_{hot}$ cannot even be inverted because the absorbance is outside the calibration range. In terms of sensing temperature uniformity, the sensor outputs inverted with $\tilde{\chi}_{H_2O}$ yield some improvement, now $\Delta T$ ranges from 175 to at least 440 K. However, uniformity detection is not strongly dependent on precise knowledge of water content.

Simply determining whether the temperature profile is uniform may not be sufficient for a sensor employed in an active control system designed to reduce temperature nonuniformities. It is advantageous for the magnitude of the sensor output to somehow scale with the degree of nonuniformity. A reasonable measure of temperature nonuniformity at the exhaust is the rms deviation in the temperature profile, that is,

$$T_{rms} \equiv \sqrt{\frac{1}{L}\int_0^L [T(x) - \tilde{T}]^2 \, dx} \tag{10}$$

The $T_{rms}$, due to its dependence on the square of the deviation, is more sensitive to the extremes in the temperature profile. Similarly, the turbine blade is more susceptible to the extremes in temperature to which it is subjected. Therefore, we investigated the relationship between the differential sensor output $\Delta T$ and $T_{rms}$ for the same temperature profiles tested earlier. The results are shown in Fig. 7. Based on the current results, there is a nearly monotonic relationship between the differential sensor output and the rms temperature deviation. Thus, the sensor proposed here could be used in the feedback loop of an active control system. The control system would simply try to minimize the output signal from the sensor, thereby minimizing the temperature nonuniformity.

## Conclusions

The IR absorption spectra of the exhaust gases of a turbine engine combustor were modeled to simulate the behavior of a sensor for monitoring water mole fraction and temperature uniformity in the combustor exhaust plane. It is intended that this line-of-sight absorption sensor would be employed in an active control system. Unlike most sensors previously proposed, the current approach would employ broadband IR sources, or perhaps a single source with a tunable bandpass filter.

Both path-integrated water content and temperature uniformity across the combustor exhaust can be monitored by a sensor using as few as three measurements between 3800 and 4100 cm$^{-1}$ (2.63–2.38 $\mu$m). In this region, the absorption is dominated by water, with little interference from the other gases that comprise the bulk of the combustor exhaust. In addition, interferences associated with dirty optics and particle extinction can be assessed at nearby wavelengths that have little water absorption. At the wavelengths chosen, expected absorbance values are between 0.02 and 0.1 for the conditions tested.

Overall water content in the exhaust is monitored at a wavelength with an absorbance that weakly depends on temperature. Based on the simulations, water measurements in a uniform mixture, inferred from a simple linear relation between mole fraction and absorbance and uncorrected for temperature dependence, would have an accuracy of about 10% over a broad range of temperatures (1000–2000 K) and water levels. Based on background absorption measurements near 4300 cm$^{-1}$ and an estimate of $10^{-3}$ in absorbance for the resolution of the sensor, mole fraction results would have a 1–2% relative resolution. In the presence of various exhaust profiles, the sensor output tends to fall between the (true) density-averaged and simple path-averaged values of water mole fraction. The simulated sensor approach achieved a relative accuracy typically better than 10%. Thus, the sensor could be used in a number of control systems that require a rapid determination of general combustor health.

Approaches for monitoring temperature uniformity were also demonstrated and involved comparison of measurements at two wavelengths, one sensitive to cold gases (3816 cm$^{-1}$) and the other sensitive to hot gases (4104 cm$^{-1}$). The difference in the temperatures inferred from these measurements is a measure of the temperature uniformity. According to the simulation results, a sensor based on this approach should be easily able to identify a nonuniform exhaust profile and even provide a reasonable measure of the amount of (rms) deviation from a uniform profile. Based on the behavior of the absorbance from the cold wavelength, a sensor based on this approach may also be able to discriminate profiles containing excessive amounts of unmixed (cold) air from those with less pronounced cold excursions.

The sensor approach described here is not limited to the three frequencies chosen in this work. If there are inaccuracies or missing transitions in the HITEMP database, there should still be some regions that behave like those used here. Also for changes in expected operating conditions, for example, pressure and average temperature, we should expect other center frequencies to have better sensitivity than the current choices. Thus, an engine sensor required to operate over a very large range of temperatures, pressures, and fuel/air ratios would either require many light sources or a broadly tunable IR source or filter. Similarly, the general method employed for monitoring temperature uniformity could also be

applicable to narrowband (diode laser) approaches if similar temperature-dependent and temperature-independent wavelengths can be identified.

## Acknowledgments

This work was partially supported under a National Science Foundation CAREER award with F. Fisher as the Technical Monitor, and an Army Research Office Multidisciplinary University Research Initiative with D. Mann as the Technical Monitor.

## References

[1]Miller, J. H., Elreedy, S., Ahvazi, B., Woldu, F., and Hassanzadeh, P., "Tunable Diode-Laser Measurements of Carbon Monoxide Concentration and Temperature in a Laminar Methane–Air Diffusion Flame," *Applied Optics*, Vol. 32, No. 30, 1993, pp. 6082–6089.

[2]Arroyo, M. P., and Hanson, R. K., "Absorption Measurement of Water Vapor Concentration, Temperature and Line-Shape Parameters Using a Tunable InGaAsP Diode Laser," *Applied Optics*, Vol. 32, No. 30, 1993, pp. 6104–6116.

[3]Allen, M. G., Miller, M. F., Sonnenfroh D. M., and Upschulte, B. L., "Diode Laser Sensors for Aeropropulsion Testing and Control," *Proceedings of the SPIE*, Vol. 3535, Society of Photo-Optical Instrumentation Engineers, Bellingham, WA, 1999, pp. 80–94.

[4]Furlong, E. R., Baer, D. S., and Hanson, R. K., "Real-Time Adaptive Combustion Control Using Diode-Laser Sensors," *Proceedings of the Twenty-Seventh Symposium (International) on Combustion*, Combustion Inst., Pittsburgh, PA, 1998, pp. 103–111.

[5]Seitzman, J. M., Tamma, R., and Vijayan, R., "Infrafred Absorption Based Sensor Approaches for High Pressure Combustion," AIAA Paper 97-0318, Jan. 1997.

[6]Rothman, L. S., Gamache, R. R., Tipping, R. H., Rinsland, C. P., Smith, M. A. H., Benner, D. C., Devi, V. M., Flaud, J.-M., Camy-Peyret, C., Perrin, A., Goldman, A., Massie, S. T., Brown, L. R., and Toth, R. A., "The HITRAN Molecular Database: Editions of 1991 and 1992," *Journal of Quantitative Spectroscopy and Radiative Transfer*, Vol. 48, Nos. 5–6, 1992, pp. 469–507.

[7]Rothman, L. S., Rinsland, C. P., Goldman, A., Massie, S. T., Edwards, D. P., Flaud, J.-M., and Perrin, A., "The HITRAN Molecular Spectroscopic Database and HAWKS (HITRAN Atmospheric Workstation): 1996 Edition," *Journal of Quantitative Spectroscopy and Radiative Transfer*, Vol. 60, No. 5, 1998, pp. 665–710.

[8]Sobelman, I. I., Vainshtein, L. A., and Yukov, E.A., "Excitation of Atoms and Broadening of Spectral Lines," Springer–Verlag, Berlin, 1981.

[9]Varghese, P. L., and Hanson, R. K., "Collisional Narrowing Effects on Spectral Lineshapes Measured at High Resolution," *Applied Optics*, Vol. 23, No. 14, 1984, pp. 2376–2385.

[10]Nagali, V., and Hanson, R. K., "Design of a Diode-Laser Sensor to Monitor Water Vapor in High-Pressure Combustion," *Applied Optics*, Vol. 36, No. 36, 1997, pp. 9518–9527.

[11]Kessler, W. J., Allen, M. G., Lo, E. Y., and Miller, M. F., "Tomographic Reconstruction of Air Temperature and Density Profiles Using Tunable Diode Laser Absorption Measurements on $O_2$," AIAA Paper 95-1953, June 1995.

[12]Arroyo, M. P., Birbeck, T. P., Baer, D. S., and Hanson, R. K., "Dual Diode-Laser Fiber-Optic Diagnostic for Water-Vapor Measurements," *Optics Letters*, Vol. 19, No. 14, 1994, pp. 1091–1093.

[13]Baer, D. S., Hanson, R. K., Newfield, M. E., and Gopaul, N. K. J. M., "Multiplexed Diode-Laser Sensor System for Simultaneous $H_2O$, $O_2$ and Temperature Measurements," *Optics Letters*, Vol. 19, No. 22, 1994, pp. 1900–1902.

[14]Upschulte, B. L., Allen, M. G., "Diode Laser Measurements of Line Strengths and Self-Broadening Parameters of Water Vapor Between 300 and 1000 K Near 1.31 $\mu$m," *Journal of Quantitative Spectroscopy and Radiative Transfer*, Vol. 59, No. 6, 1998, pp. 653–670.